Supporting Information

Dual-vacancy engineering of CuCoOOH synergistically activates lattice and adsorbed oxygen for efficient glycerol electrooxidation

Ruoxi Hong *et al.*

1. Supplementary Methods

In-situ Raman measurement.

In-situ Raman spectra were acquired using a Thermo Scientific DXR2 Raman microscope with a 532 nm laser excitation source, while the applied potential was controlled by a Corrtest CS310MA electrochemical workstation. The in-situ Raman cell featured a Teflon shell sealed with a thin, round quartz glass cover. Within this cell, the D_v-CuCoOOH sample served directly as the working electrode, while a Hg/HgO electrode (filled with 1 M KOH) and a Pt wire electrode functioned as the reference and counter electrodes, respectively. The 532 nm laser was focused onto the sample through a 10× objective lens. To minimize the interference from O_2 bubbles and ensure an unblocked optical path, the electrolyte (1 M KOH with or without 0.1 M glycerol) was continuously circulated using a peristaltic pump. All Raman spectra were collected at various potentials (1.00 to 1.60 V_{RHE} in 0.05 V increments) after holding at each potential for 60 s.

In situ ATR- FTIR measurement.

Attenuated total reflection surface-enhanced infrared absorption spectroscopy (ATR-SEIRAS) data were obtained using a BRUKER INVENIO S spectrometer equipped with a thermoelectrically cooled MCT detector. Spectroscopic measurements were conducted in a custom-designed spectro-electrochemical cell supplied by Yuanfang Instrument Co., Ltd. (Shanghai, China), Ltd. In situ ATR-SEIRAS working electrodes were fabricated following established protocols. Specifically, a thin gold film was electrochemically deposited onto the reflecting surface of a silicon prism, which was subsequently drop-cast with catalyst ink. The D_v-CuCoOOH electrocatalyst ink was prepared by dispersing 5 mg of catalyst powder and 50 μL of Nafion solution within 1 mL of a solvent mixture comprising deionized water and ethanol

in a 1:1 volume ratio. The catalyst-coated gold film served as the working electrode. A platinum wire and a Hg/HgO electrode functioned as the counter and reference electrodes, respectively, during all electrochemical measurements. The electrolyte comprised 0.1 M KOH with 0.1 M glycerol. Prior to spectral acquisition, the gold film was activated via cyclic voltammetry in 0.5 M H_2SO_4, scanned from 0 to 1.45 V_{RHE} at 100 mV s^{-1} for three cycles. Linear sweep voltammetry was conducted over a potential window of 0.87 to 1.49 V_{RHE}, without iR compensation.

2. Supplementary Figures

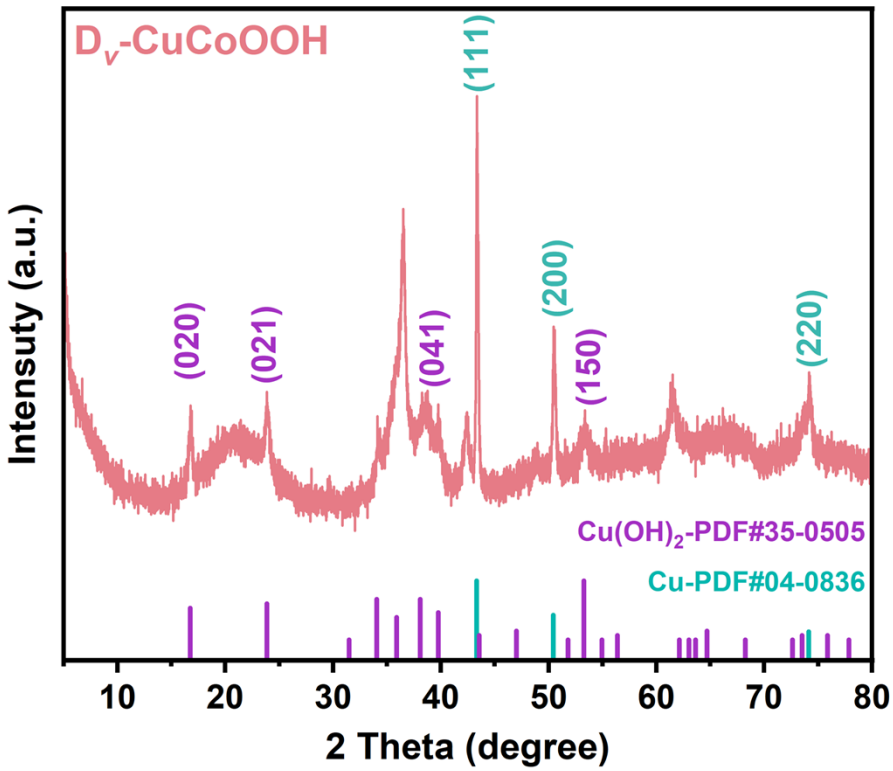

Fig. S1. XRD pattern of D_v-CuCoOOH.

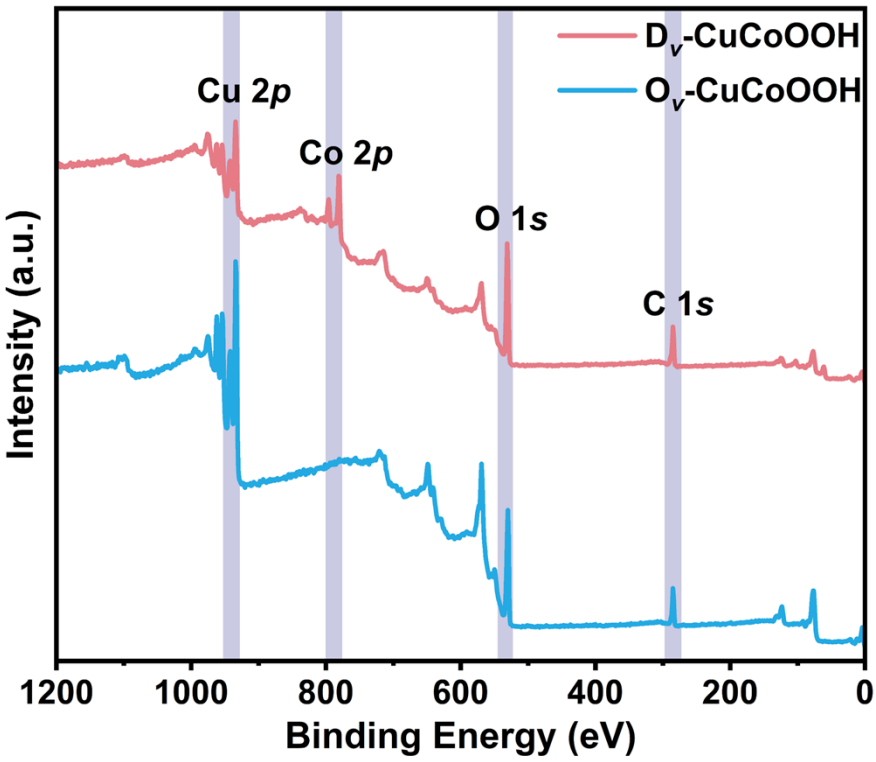

Fig. S2. The survey XPS spectrums of D_v-CuCoOOH and O_v-CuCoOOH.

Note: The Co 2*p* signal appears weak in the survey spectra of O_v-CuCoOOH due to the fast scan speed and high pass energy of the survey mode. For detailed identification of the Co species, the high-resolution Co 2*p* spectra are provided, as shown in Fig. 2a.

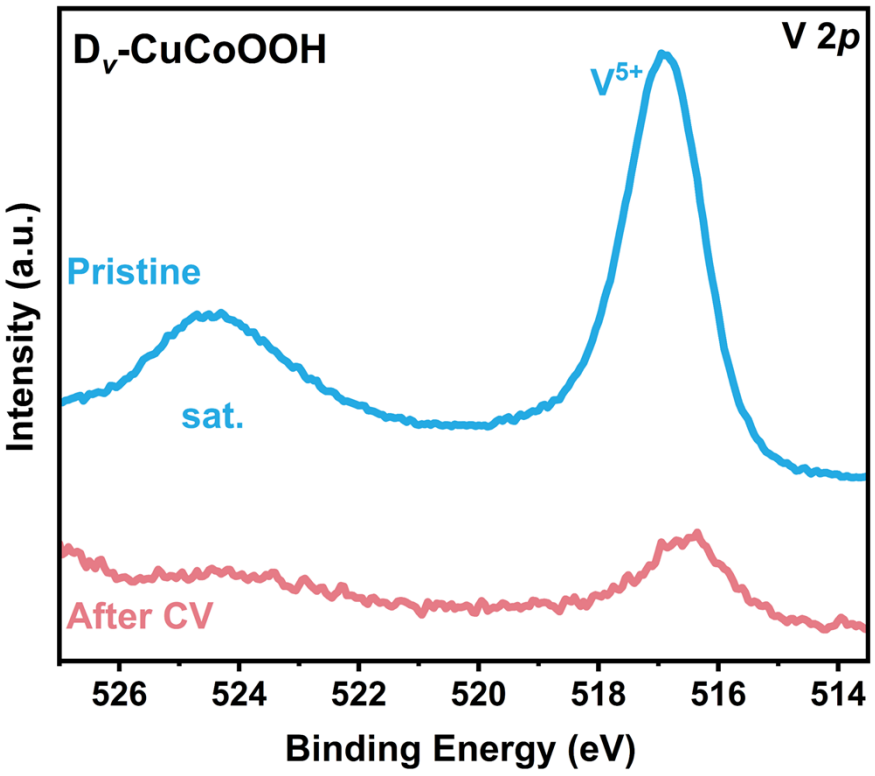

Fig. S3. XPS spectra of V 2*p* before and after CV activation.

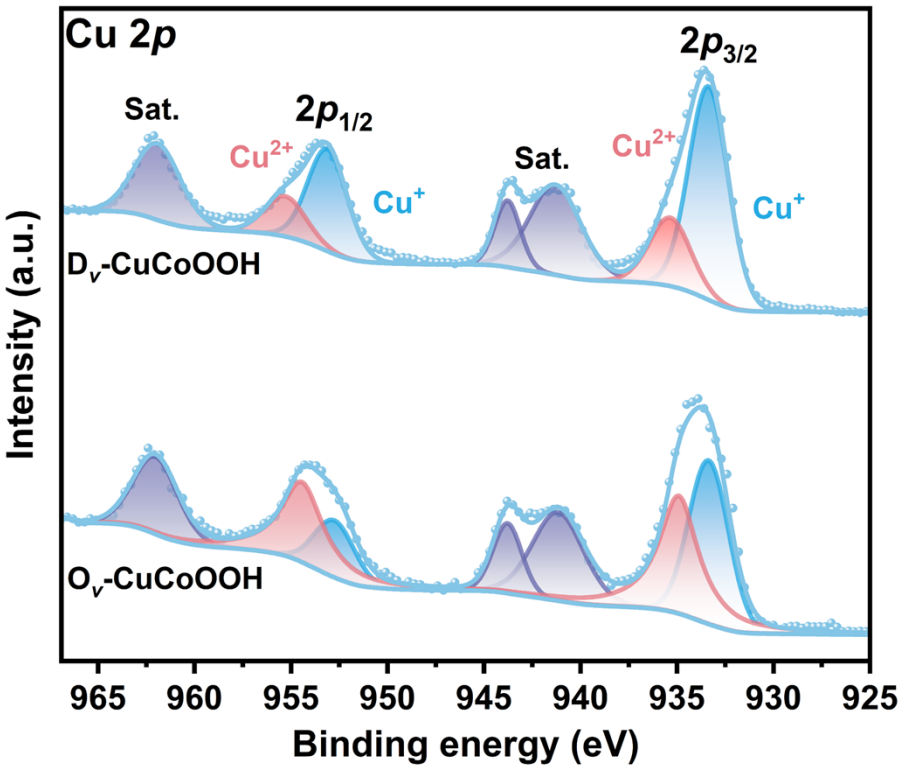

Fig. S4. Cu 2*p* XPS spectra of D_v-CuCoOOH and O_v-CuCoOOH.

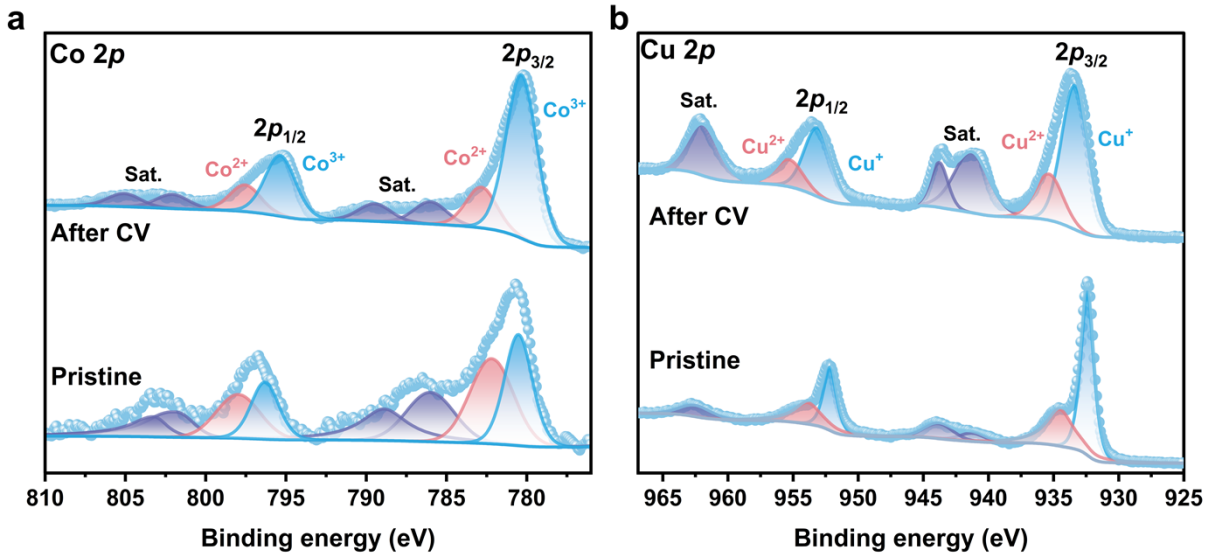

Fig. S5. XPS spectra of (a) Co and (b) Cu 2*p* before and after CV activation.

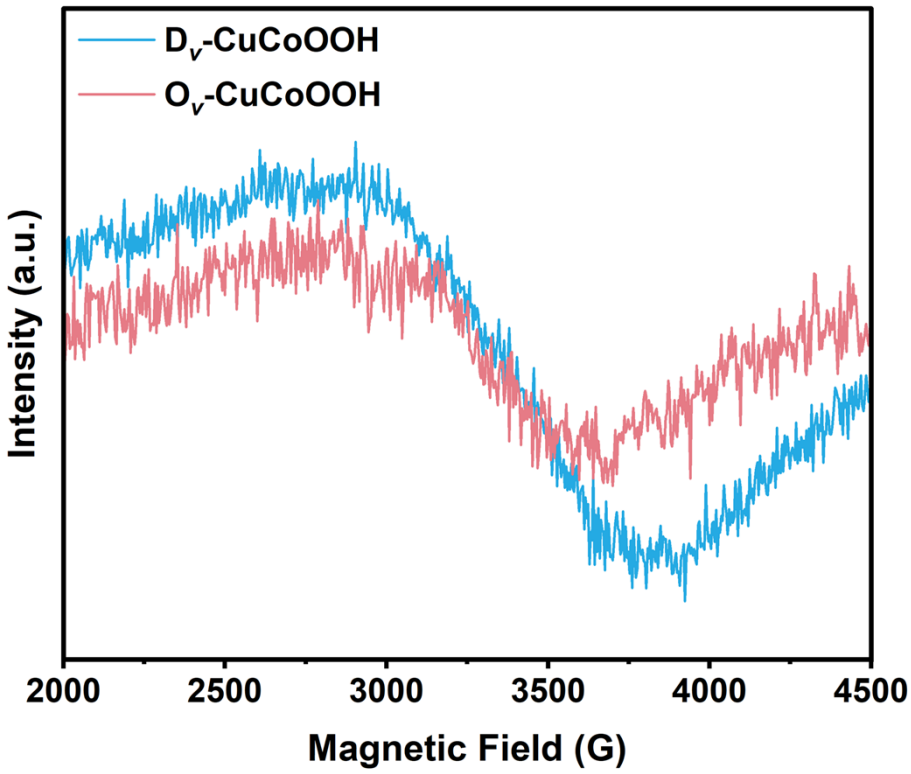

Fig. S6. EPR spectra of D_v-CuCoOOH and O_v-CuCoOOH.

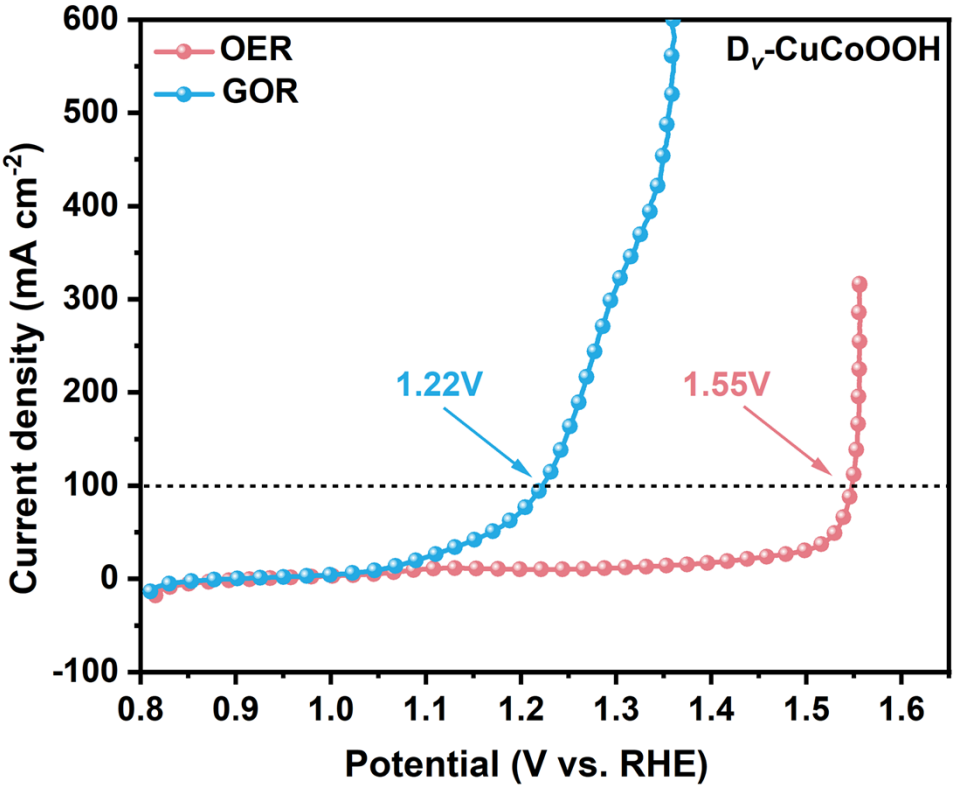

Fig. S7. LSV curves of Dv-CuCoOOH for the OER in 1 M KOH and the GOR in 1.0 M KOH with 0.1 M glycerol.

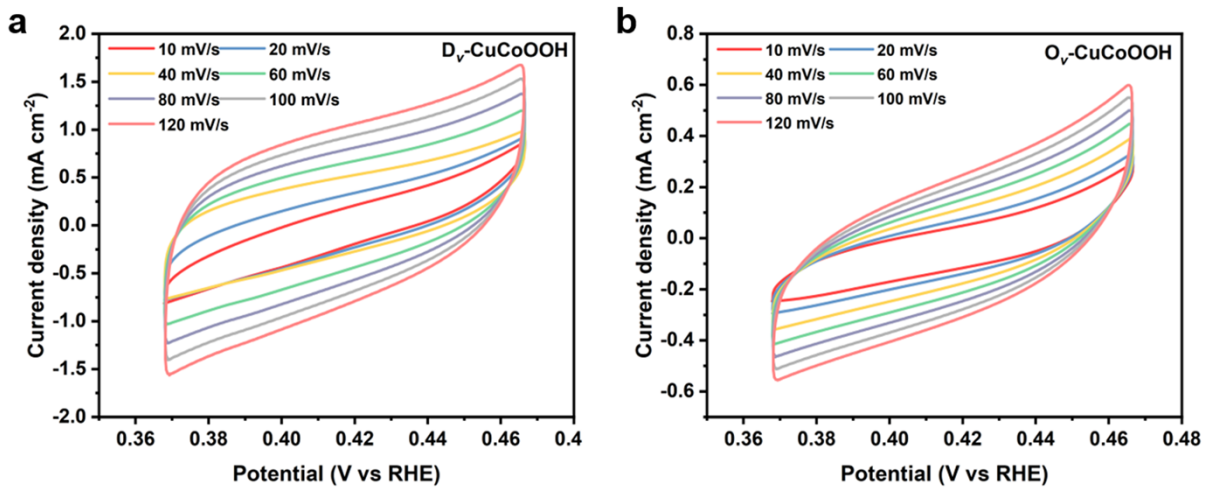

Fig. S8. CV curves of (a) D_v-CuCoOOH and (b) O_v-CuCoOOH.

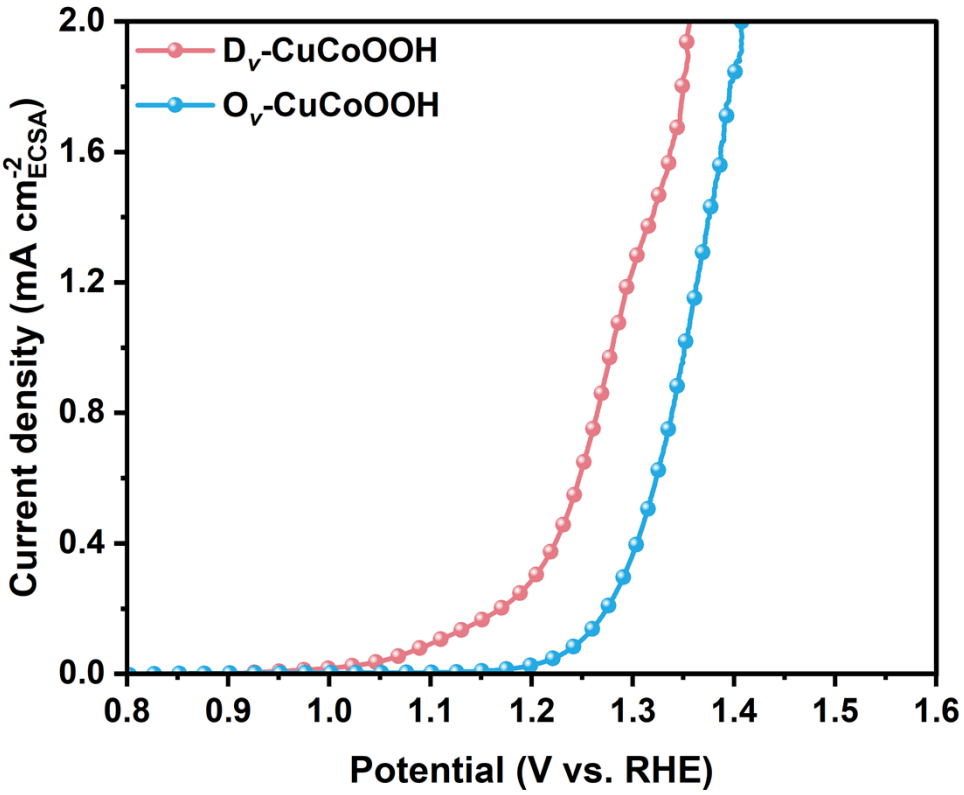

Fig. S9. LSV curves normalized by ECSA.

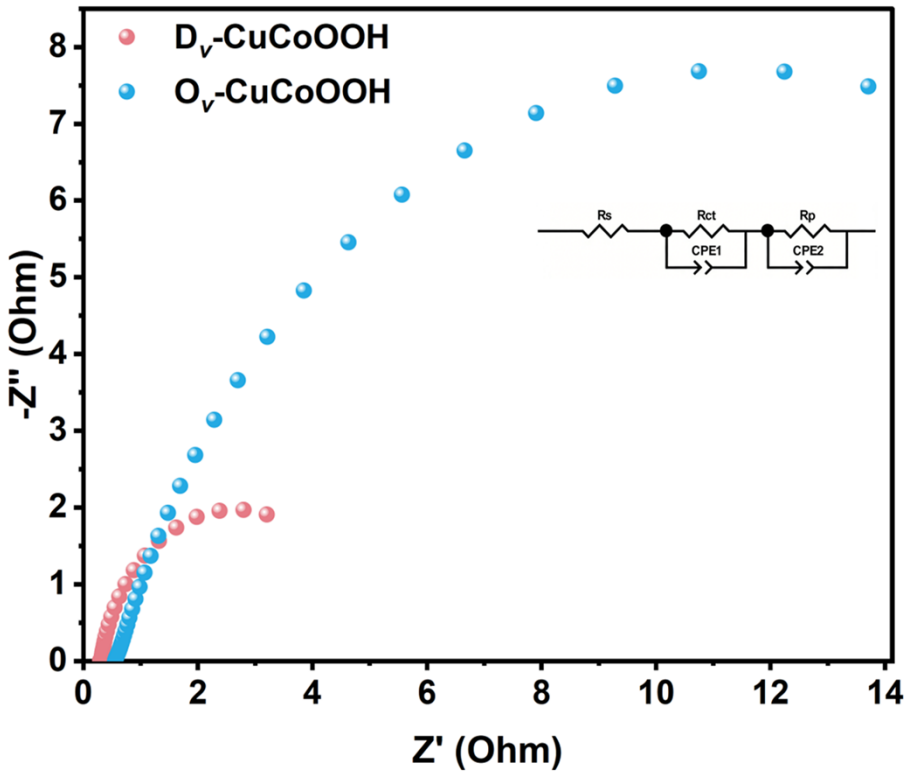

Fig. S10. Nyquist plots of D_v-CuCoOOH and O_v-CuCoOOH collected at a constant potential of 1.45 V_{RHE} with 0.1 M glycerol.

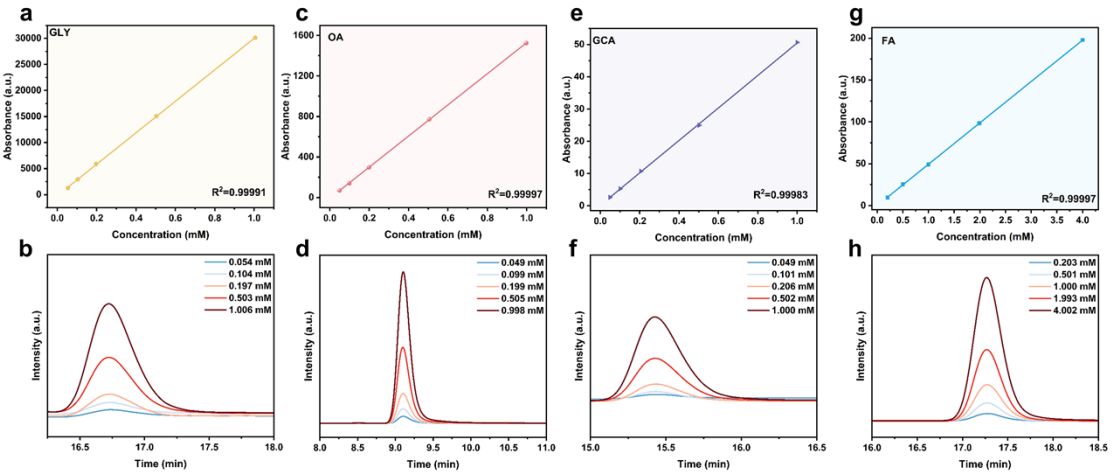

Fig. S11. HPLC chromatograms of glycerol and intermediate products derived from the glycerol oxidation in various concentrations, and their corresponding calibration curves used to quantify the concentrations of the respective molecules from the chromatograms: (a, b) glycerol (GLY), (c, d) oxalic acid (OA), (e, f) GCA, and (g, h) FA.

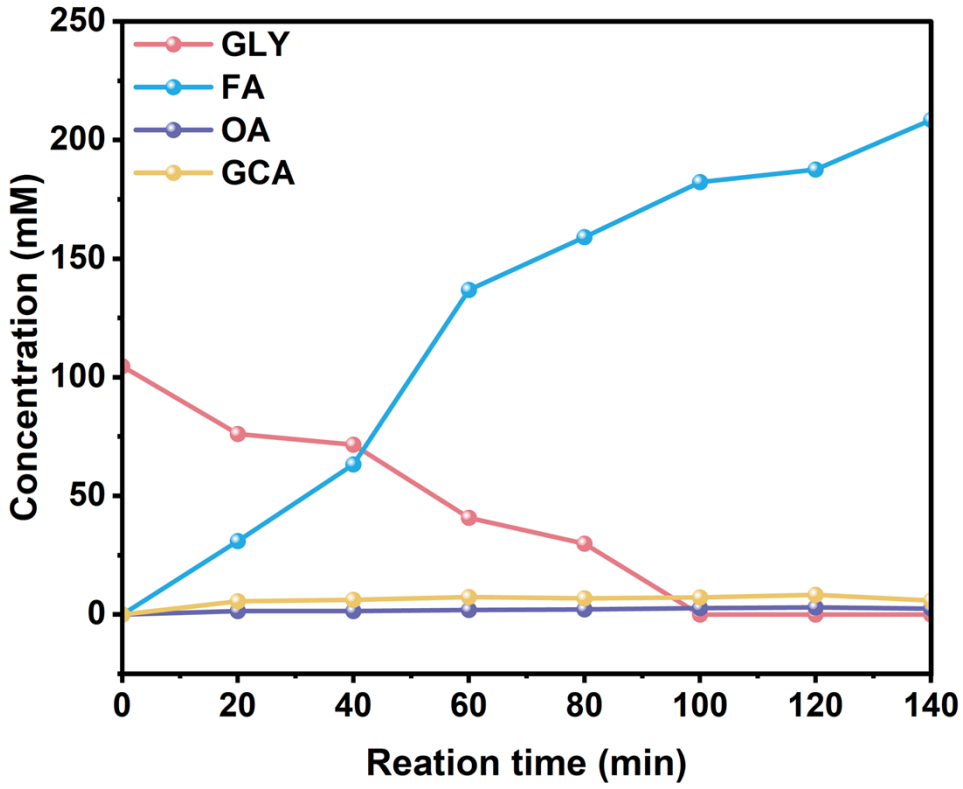

Fig. S12. Concentration of glycerol, FA, OA, and GCA as a function of reaction time (the chronoamperometric test was performed at 1.34 V_{RHE}.

Note: The electrolyte was sampled at 20, 40, 60, 80, 100, 120, and 140 min to track the evolution of reaction intermediates.

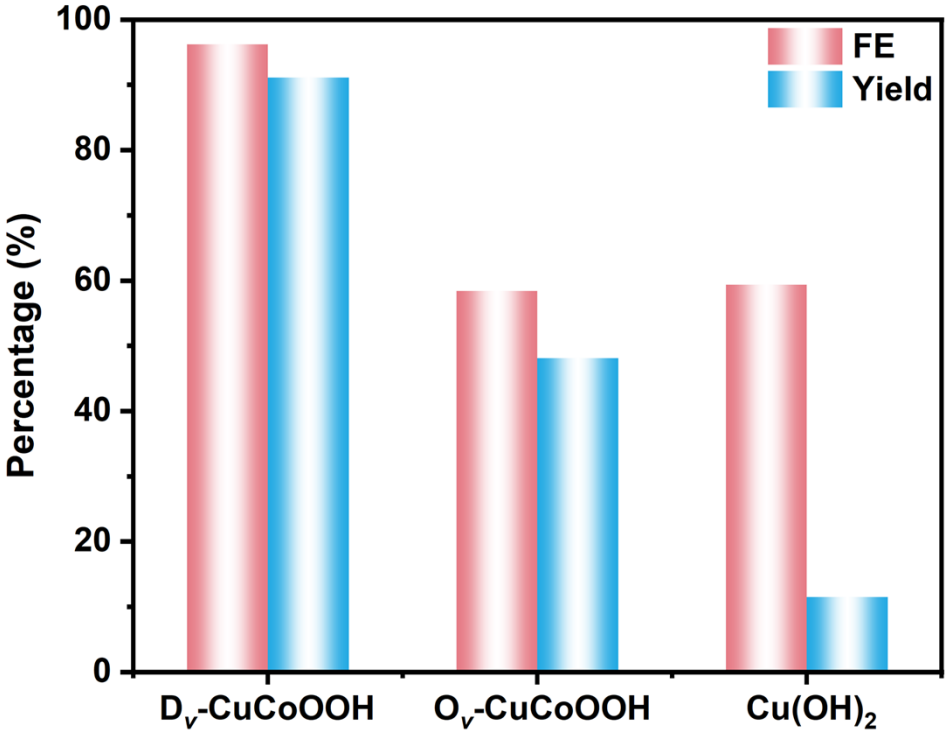

Fig. S13. FE and FA yield of the three catalysts at 1.34 V_{RHE}.

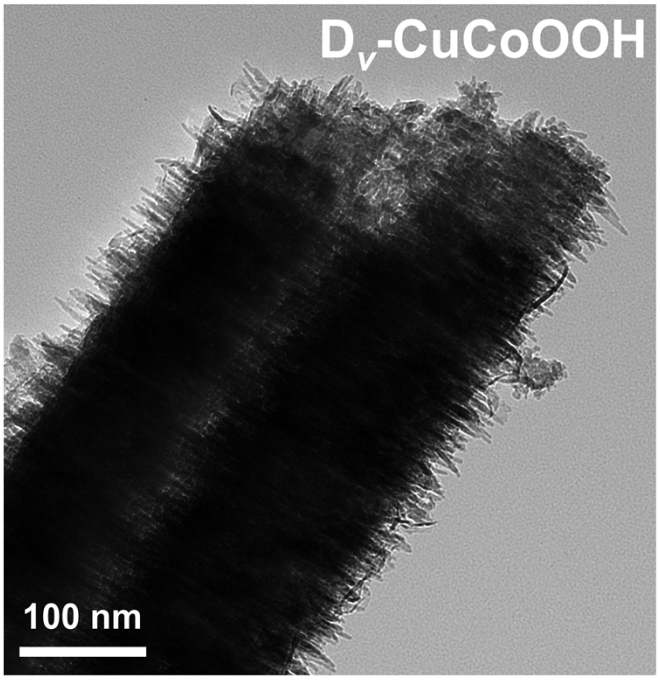

Fig. S14 TEM image of the post D_v-CuCoOOH.

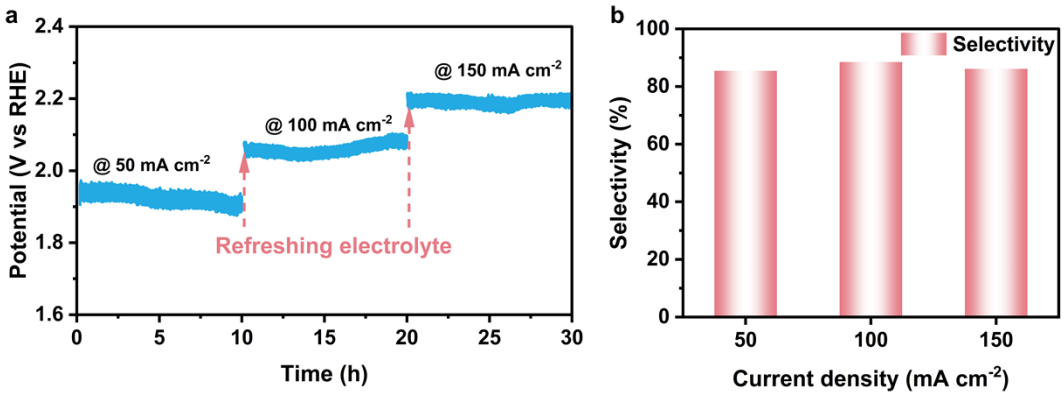

Fig. S15. (a) Stability test and (b) FE of FA for the D_v-CuCoOOH-based MEA electrolyser under constant current operation at different current densities.

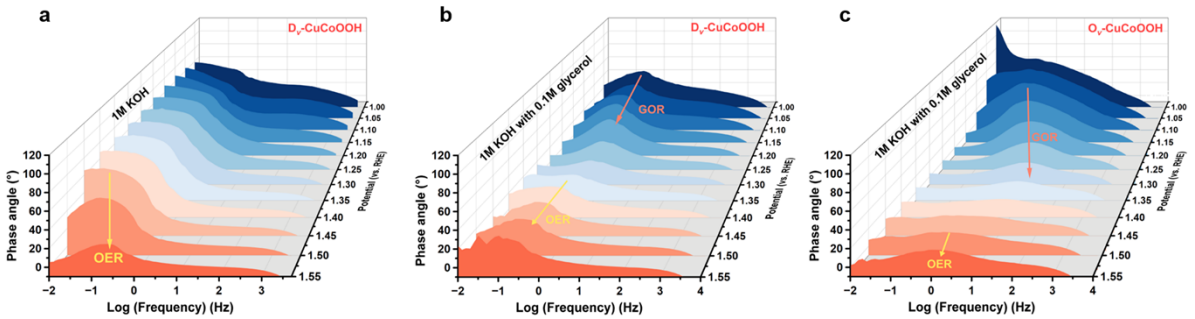

Fig. S16. In situ EIS of in situ electrochemical impedance spectra for (a) D_v-CuCoOOH under OER conditions, (b) D_v-CuCoOOH and (c) O_v-CuCoOOH under GOR conditions.

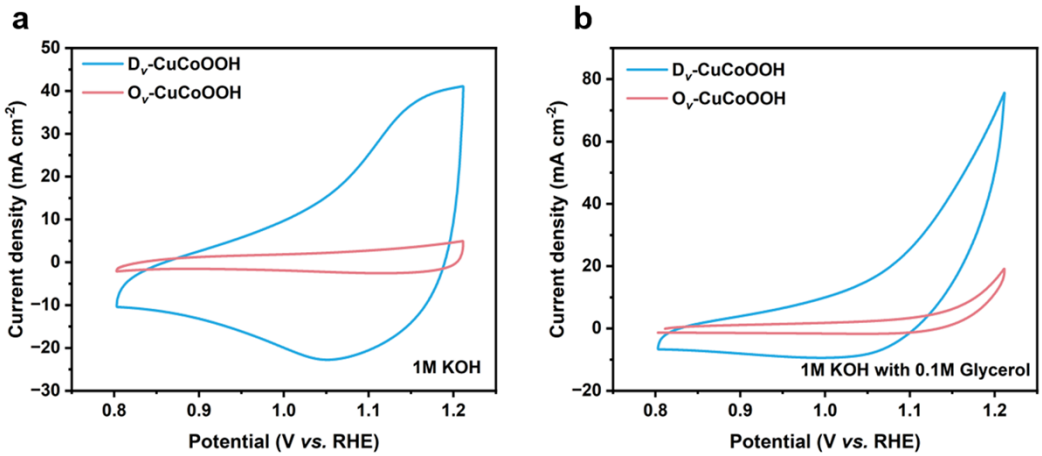

Fig. S17. CV curves of D_v-CuCoOOH and O_v-CuCoOOH in (a) 1.0 M KOH and (b) 1.0 M KOH with 0.1 M glycerol.

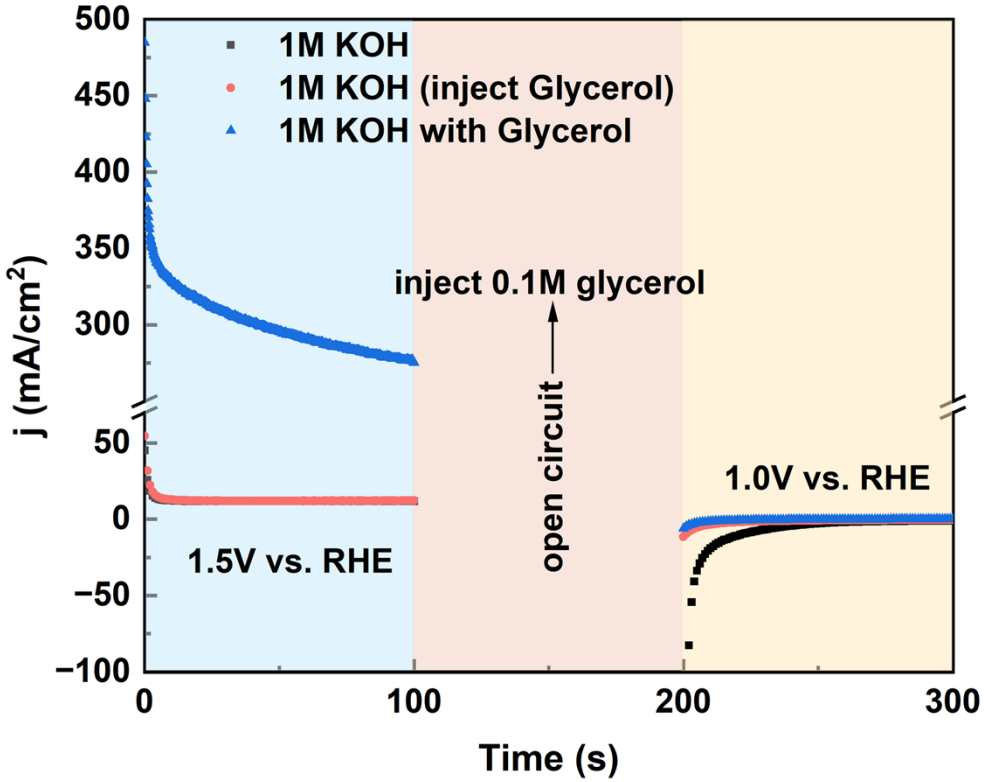

Fig. S18. Multi-potential steps curves of D_v-CuCoOOH.

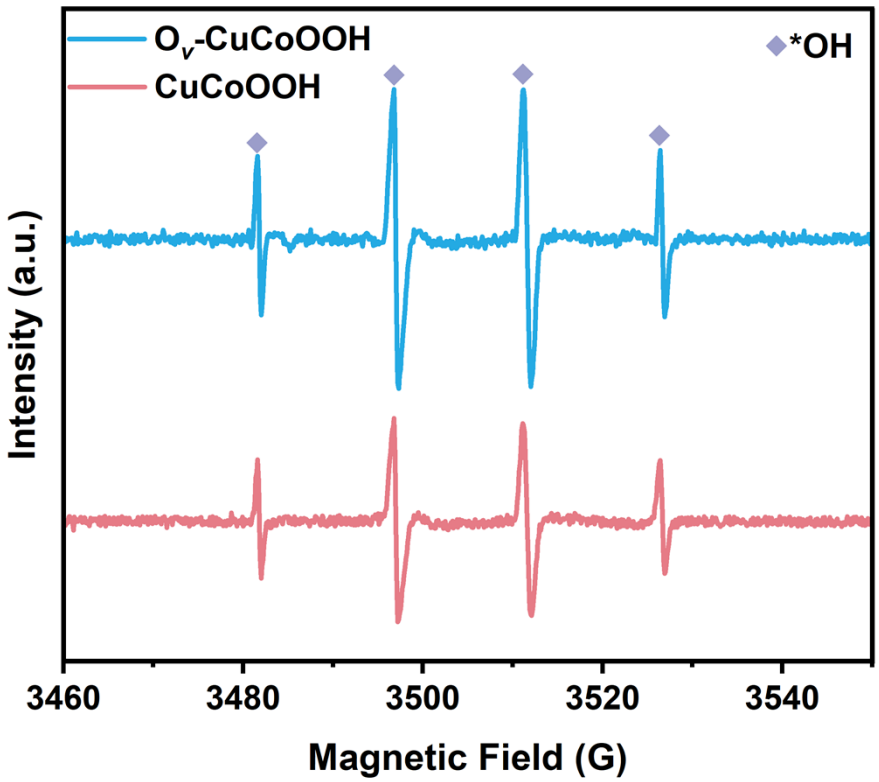

Fig. S19. EPR spectroscopy using DMPO as the trapping agent.

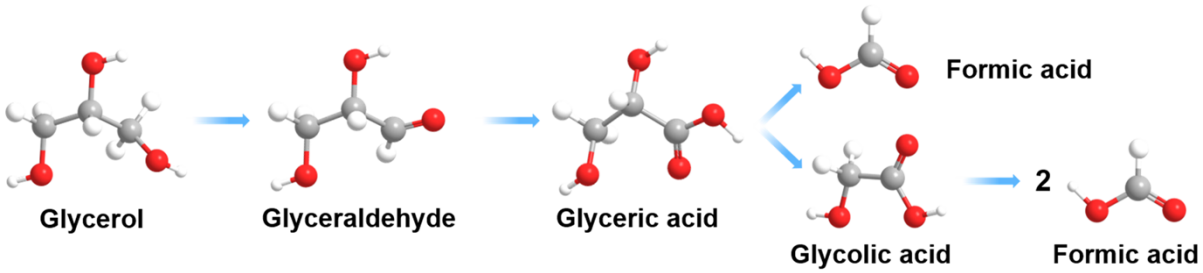

Fig. S20. Primary pathway for GOR to FA under alkaline conditions.

3. Supplementary Tables

Table S1. The ratio of the different components in the corresponding deconvoluted Co 2*p* and Cu 2*p* XPS spectra.

Samples	Co^{2+}	Co^{3+}	Cu^{+}	Cu^{2+}
D_v-CuCoOOH	19.9%	80.1%	75.7%	24.3%
O_v-CuCoOOH	27.7%	72.3%	49.7%	50.3%

Table S2. Comparison of Co^{3+} and Cu^{+} proportions in D_v-CuCoOOH before and after CV activation by XPS spectra analysis

Samples	Co^{3+}	Co^{2+}	Cu^{2+}	Cu^{+}
Pristine V-CuCoOOH	46.2%	53.8%	36.5%	63.5%
D_v-CuCoOOH	80.1%	19.9%	24.3%	75.7%

Table S3. The ratio of the different components in the corresponding deconvoluted O 1*s* XPS spectra.

Samples	O^{2-} in oxide	O in OH^-	H_2O
D_v-CuCoOOH	35.5%	53.0%	11.5%
O_v-CuCoOOH	54.4%	18.9%	26.7%

Table S4. The comparison of GOR activity of Dv-CuCoOOH with other non-noble-metal-based electrocatalysts in 1 M KOH with 0.1 M glycerol.

Catalyst	Potential at 10 mA cm^{-2} (V_{RHE})	Ref.
D_v-CuCoOOH	1.05	This work
CoNiCuMnMo/CC	1.25	1
$NiCo_3O_4$	1.13	2
NC/Ni-Mo-N/NF	1.16	3
Ni-Mo-N/CFC	1.30	4
$CuCo_2O_x$(HV_o-S)	1.32	5
CuO@$NiBiO_x$	1.45	6
CoO/CFP	1.32	7
$CoSe_2$/CC	1.23	8
$FeCoNiCrMnS_2$/CC	1.10	9
$Ni_3(HHTQ)_2$	1.36	10

4. Supplementary References

1. L. F. Fan, Y. X. Ji, G. X. Wang, J. X. Chen, K. Chen, X. Liu and Z. H. Wen, High Entropy Alloy Electrocatalytic Electrode toward Alkaline Glycerol Valorization Coupling with Acidic Hydrogen Production, *J. Am. Chem. Soc.*, 2022, **144**, 7224–7235.
2. W. Luo, H. Tian, Q. Li, G. Meng, Z. Chang, C. Chen, R. Shen, X. Yu, L. Zhu, F. Kong, X. Cui and J. Shi, Controllable Electron Distribution Reconstruction of Spinel $NiCo_2O_4$ Boosting Glycerol Oxidation at Elevated Current Density, *Adv. Funct. Mater.*, 2023, **34**, 2306995.
3. Y. Xu, M. Y. Liu, S. Q. Wang, K. L. Ren, M. Zwang, Z. Q. Wang, X. N. Li, L. Wang and H. J. Wang, Integrating electrocatalytic hydrogen generation with selective oxidation of glycerol to formate over bifunctional nitrogen-doped carbon coated nickel-molybdenum-nitrogen nanowire arrays, *Appl. Catal., B*, 2021, **298**, 120493.
4. Y. Li, X. Wei, L. Chen, J. Shi and M. He, Nickel-molybdenum nitride nanoplate electrocatalysts for concurrent electrolytic hydrogen and formate productions, *Nat. Commun.*, 2019, **10**, 5335.
5. L. Wu, Q. Wu, Y. Han, D. Zhang, R. Zhang, N. Song, Y. Fang, H. Liu, M. Wang, J. Chen, A. Du, K. Huang and X. Yao, Constructing Asymmetric Defects Pairs in Electrocatalysts for Efficient Glycerol Oxidation, *J. Am. Chem. Soc.*, 2025, **147**, 18033–18043.
6. T. H. H. Le, Y. Zuo, M. Chatti, M. Rizzo, A. Griesi, A. Annamalai, S. Lauciello, L. Leoncino, M. Prato, S. Dante, I. Kriegel, G. Divitini, M. Ferri and L. Manna, Coupling of CuO@$NiBiO_x$ Catalyzed Glycerol Oxidation to Carbon Dioxide Reduction Reaction for Enhanced Energy Efficiency, *Angew. Chem., Int. Ed.*, 2025, **64**, e202502617.
7. N. Xi, Y. Zang, X. Sun, J. Yu, M. Johnsson, Y. Dai, Y. Sang, H. Liu and X. Yu, Polyhedral Coordination Determined Co-O Activity for Electrochemical Oxidation of Biomass Alcohols, *Adv. Energy Mater.*, 2023, **13**, 2301572.
8. G. X. Wang, J. X. Chen, K. K. Li, J. H. Huang, Y. C. Huang, Y. J. Liu, X. Hu, B. S. Zhao, L. C. Yi, T. W. Jones and Z. H. Wen, Cost-effective and durable electrocatalysts for Co-electrolysis of CO_2 conversion and glycerol upgrading, *Nano Energy*, 2022, **92**,

106751.

9. P. Wang, G. Wang, K. Chen, W. Pan, L. Yi, J. Wang, Q. Chen, J. Chen and Z. Wen, High-power hybrid alkali-acid fuel cell for synchronous glycerol valorization implemented by high-entropy sulfide electrocatalyst, *Nano Energy*, 2023, **118**, 108992.

10. Y. Luo, M. Beerbaum, S. Röher, S. A. Salout, V. Bon, Y. Lu, L. Shupletsov, A. De, X. Feng, I. M. Weidinger, T. Kühne, A. H. Khan, I. Senkovska and S. Kaskel, Two-dimensional conjugated metal-organic frameworks as electrocatalysts for boosting glycerol upgrading coupled with hydrogen production, *Angew. Chem., Int. Ed.*, 2025, **64**, e202502425.